Soft Materials

ISSN: 1539-445X (Print) 1539-4468 (Online) Journal homepage: http://www.tandfonline.com/loi/lsfm20

Multilayered electrospun nanofibrous scaffolds for tailored controlled release of embelin

Pablo R. Cortez Tornello, Gabriela E. Feresin, Alejandro Tapia, Teresita R. Cuadrado & Gustavo A. Abraham

To cite this article: Pablo R. Cortez Tornello, Gabriela E. Feresin, Alejandro Tapia, Teresita R. Cuadrado & Gustavo A. Abraham (2018) Multilayered electrospun nanofibrous scaffolds for tailored controlled release of embelin, Soft Materials, 16:1, 51-61, DOI: 10.1080/1539445X.2017.1398173

To link to this article: https://doi.org/10.1080/1539445X.2017.1398173

SOFT MATERIALS
2018, VOL. 16, NO. 1, 51–61
https://doi.org/10.1080/1539445X.2017.1398173

Taylor & Francis
Taylor & Francis Group

Multilayered electrospun nanofibrous scaffolds for tailored controlled release of embelin

Pablo R. Cortez Tornello[a], Gabriela E. Feresin[b], Alejandro Tapia[b], Teresita R. Cuadrado[a], and Gustavo A. Abraham[a]

[a]División Polímeros Biomédicos, Instituto de Investigaciones en Ciencia y Tecnología de Materiales, INTEMA (UNMdP-CONICET), Mar del Plata, Argentina; [b]Instituto de Biotecnología, Facultad de Ingeniería, Universidad Nacional de San Juan, San Juan, Argentina

ABSTRACT

Polymeric electrospun meshes are highly attractive as versatile platforms for numerous biomedical applications, tissue engineering, biosensors, and controlled release of bioactive agents. Herein, we describe the preparation and characterization of multilayered nanofibrous poly(ε-caprolactone) scaffolds with different embelin content by electrospinning technique. In vitro release in physiological and acidic pH and kinetic analysis were performed. The results show that it is possible to modulate the release profile depending on the number and thickness of layers added to drug-loaded scaffold that acts as an embelin reservoir. Electrospun multilayered scaffolds present characteristics, morphology and release profiles that could be very attractive for use as embelin controlled release systems.

ARTICLE HISTORY
Received 11 September 2017
Accepted 25 October 2017

KEYWORDS
Drug release; embelin; electrospinning; multilayered scaffolds; nanofibers

Introduction

Electrospun nanofibrous scaffolds have received a considerable attention of many biomaterial researchers as highly versatile platforms for a broad range of biomedical applications (1,2). Tissue engineering (3,4), biomolecules immobilization (5,6), wound healing (7,8), vascular grafts (9–11), controlled delivery of therapeutic agents (12–14) and barriers for the prevention of post-operative induced adhesion (15,16) are among the most explored applications. Electrospun micro- and nanofibers have structural and functional characteristics that improve mass transfer and drug release efficiency making them very attractive as drug delivery systems (17,18).

Embelin is a natural benzoquinone isolated from species of the *Myrsinaceae* and *Oxalidaceae* families, and it known as *Vidang* in Ayurvedic medicine (19–21). Embelin has a wide range of pharmacological activities, including anthelmintic, antifertility, antitumor, antimicrobial, antifungal, and analgesic activities (22,23). In previous works, the authors were the first in reporting the preparation and characterization of poly(ε-caprolactone) (PCL) scaffolds containing embelin obtained by solution casting and electrospinning techniques (24), and microparticles fabricated by electrohydrodynamic atomization and emulsion-solvent evaporation techniques (25). The release characteristics of these embelin-loaded systems were completely described and analyzed.

PCL is an aliphatic and biocompatible polyester that exhibits a long degradation time under physiological conditions (2 years), owing to its hydrophobic character and semi-crystalline structure. These properties are attractive for long-term applications in drug delivery.

Drugs can be incorporated into electrospun polymeric nanofibers by using different strategies (26). The drug can be dispersed homogeneously on polymeric fiber, completely encapsulated in a core, randomly distributed in aggregates or located in fibrous meshes surface. In some cases, significant burst release can take place during the first stage of release process (27). Burst release can be considered undesirable in some applications for tissue engineering, but it is necessary in case of infectious diseases that could take place during the first hours after surgical procedures. In order to decrease or avoid this initial release, some approaches such as the use of polymer blends or copolymers (28,29), surface modification of fibers (30), and polymer coatings (31), were explored.

In this work, embelin-loaded scaffolds with different embelin content and multilayered nanofibrous systems were prepared and completely characterized by different techniques. *In vitro* embelin release of these structures was studied in different pH and a kinetic analysis of the release profiles was performed. Multilayered scaffolds were explored as an interesting strategy to modulate both the burst effect and profiles as well as to tailor the dosage of different therapies.

CONTACT Gustavo A. Abraham gabraham@fi.mdp.edu.ar Instituto de Investigaciones en Ciencia y Tecnología de Materiales, INTEMA (UNMdP-CONICET), Av. Juan B. Justo 4302, B7608FDQ Mar del Plata, Argentina.
Supplemental data for this article can be accessed on the publisher's website.

Experimental

Materials

Embelin (2,5-dihydroxy-3-undecil-2,5-cyclohexadiene-1,4-dione) (Mw 294.39 g mol^{-1}) was obtained from *Oxalis erythrorhiza Gillies ex Hooker et Arnott* (Oxalidaceae) (19,32) collected in the province of San Juan, Argentina, following the procedure described by Feresin et al. (20). Poly(ε-caprolactone) (PCL, Mw 80,000 g mol^{-1}), dimethylformamide (DMF, 99%) and dichloromethane (DCM, 99.5%) were purchased from Aldrich Chemical Co. (St. Louis, MO, USA). Analytical grade solvents were used without further purification. Phosphate buffered saline (PBS, 100 mM, pH = 7.4) and phosphate-citrate buffer (PCB, 100 mM, pH = 5.0) were also acquired from Aldrich Chemical Co. (St. Louis, MO, USA).

Preparation of nanofibrous embelin-loaded PCL scaffolds

PCL solutions (18% w/v) were prepared by dissolving PCL pellets in a DCM:DMF solvent mixture (50:50 by volume) under magnetic stirring at room temperature. For drug-loaded formulations, 1.5, 3 and 5% w/w of embelin with respect to PCL was added to the polymer solutions, and samples were named $PCLE_{1.5}$, $PCLE_{3,}$ and $PCLE_5$, respectively. The flask was protected from light during the dissolution process, and the mixture was maintained under magnetic stirring at room temperature, until processing.

The amount of embelin was selected to assure the minimum inhibitory concentration index (MIC) in each type of sample. Embelin activity against *Trypanosoma cruzi trypomastigotes* was reported at a MIC of 100 mg ml^{-1} (20) whereas that bactericidal activity against Gram-positive organisms and bacteriostatic activity against Gram-negative organisms was found with a MIC below 100 mg ml^{-1} (33). Based on the above reports, the prepared meshes contained an amount of embelin enough to act as effective drug delivery systems with bactericidal and trypanocidal activity.

Solutions were loaded into a 10 ml syringe connected to a polyamide tube. A blunt 18-gauge stainless steel needle was attached to the end of the tube and use as a nozzle. The flow rate was controlled by using a programmable syringe pump (Activa A22 ADOX S.A., Ituzaingó, Argentina). A high-voltage power source (ES30P, Gamma High Voltage Research Inc., Ormond Beach, FL, USA) was used to charge the solution by attaching the emitting electrode of positive polarity to the nozzle, and the grounding one to the aluminum collecting foil. All experiments were carried out at 20°C and 50% relative humidity. Electrospinning was conducted during 6 h using the following processing parameters: 20 kV applied voltage, 12 cm needle-to-collector distance, and 0.6 ml h^{-1} a solution feeding-rate. These parameters were fixed after several experiments to allow a stable cone-jet regime during all the electrospinning process. The electrospun meshes were dried under vacuum at room temperature to fully eliminate the residual solvent and were stored in a desiccator.

Preparation of nanofibrous multilayered PCL scaffolds

Multilayered scaffolds were prepared by using sequential deposition of layers. Bi- and three-layered meshes with different thickness were obtained by using 10 and 60 min deposition times of PCL layers keeping constant a $PLCE_3$ layer. In such way that, bi-layered scaffolds (B10 and B60), and three-layered ones (sandwich-like structures with a central layer of embelin-loaded nanofibers, T10 and T60) were obtained. The thickness of $PCLE_3$ layer was 10 μm, while that the additional layers of PCL were 0.3 μm and 2 μm for 10 min and 60 min deposition, respectively.

Polymer and embelin characterization

The morphology of meshes was examined by scanning electron microscopy (SEM, JEOL JSM6460 LV, Peabody, MA, USA) operated at 15 kV. Samples were sputter-coated with gold during 20 min in a chamber evacuated to 500 mTorr (Sputter coater, Desk II, Denton Vacuum, Moorestown, NJ, USA) before examination. Micrographs were analyzed using Image Pro Plus software to measure the mean diameter and diameter distribution. In order to obtain a meaningful statistical value, 100 randomly selected fibers per sample were measured.

Thermal properties of PCL, embelin and embelin-loaded systems were determined by differential scanning calorimetry (DSC, PerkinElmer Inc., Model Pyris 1, Waltham, MA, USA). Scans were carried out at a heating rate of 5°C min^{-1}. Thermograms were obtained under nitrogen atmosphere. Glass transition temperature was taken as the onset of the transition. The degree of crystallinity of PCL (X_C) was calculated as:

$$X_C(\%) = (\Delta H_m \text{experimental} / \Delta H_m \text{theorical}).\ 100 \quad (1)$$

where the theoretical melting heat (ΔHm) for pure high molecular weight PCL was taken as 148.05 J g^{-1} (34).

Fourier transform infrared spectroscopy (FTIR) spectra were obtained with a Nicolet 6700 (Thermo Scientific, Inc., Waltham, MA, USA) spectrometer. Attenuated total reflectance (ATR) mode was used to

record spectra over the range 4000 – 450 cm^{-1} at a resolution of 2 cm^{-1}.

X-ray diffraction (XRD) analysis was performed in a PANalytical X`Pert PRO diffractometer equipped with an X-ray source (Philips PW 1830, PANalytical BV) using CuKα radiation at 40 kV and 40 mA. Diffraction patterns were collected over 2θ range of 5°–75° with an acquisition time of 1 second at each step of 0.02°.

X-ray photoelectron spectroscopy (XPS) analysis was performed in a multi-technique system (SPECS) equipped with an X-ray dual source of Mg/Al and a hemispheric analyzer (PHOIBOS 150) operated in fixed analyzer transmission (FAT) mode at 30 eV pass energy. Mg anode operated at 100 W and pressure lower than 2.10 – 8 mbar were used. The samples were prepared over a double-sided tape and evacuated during 12 h before the analysis.

Embelin loading capacity and encapsulation efficiency

Embelin content was determined by ultraviolet-visible spectroscopy using an Agilent 8453 spectrometer (Santa Clara, CA, USA) equipped with a diode array system. A predetermined amount of sample was dissolved in DCM: DMF (1:1 by volume), and quantification was carried out observing the absorption band at λ = 296 nm. At least three measurements were performed.

The loading capacity (LC) was calculated from the ratio between the embelin mass in the mesh $(m_E)_f$ and the mesh mass $(m_P)_f$ in PCLE mesh.

$$LC\ (\%) = (m_E)_f/(m_p)_f.\ 100 \qquad (2)$$

The encapsulation efficiency (EE) was calculated as:

$$EE\ (\%) = (m_{Ef}/m_{PCLf})/(m_{Ei}/m_{PCLi}).100 \qquad (3)$$

where m_{Ef} is the mass of embelin encapsulated, m_{Ei} the initial mass of embelin, and m_{PCLf} and m_{PCLi} correspond to the final and initial mass of PCL, respectively.

Embelin release measurements

Drug release from embelin-loaded samples (10 discs of 10 mm in diameter) was measured in glass flasks containing 200 ml PBS pH = 7.4 or PCB pH = 5.0 at 37°C. Stirring was performed with an orbital shaker at 150 rpm. A volume of 1 ml was extracted each 1 h during the first 12 h, and then each 24 h during 18 days. A total of 30 extractions were performed. After each extraction, 1 ml of fresh solvent was added. The total volume extracted was lower than 15% of the solution volume. All the assays were performed in triplicate. The concentration of embelin was determined by ultraviolet-visible spectroscopy measuring the absorption band at λ = 330 nm for PBS and λ = 349 nm for PCB.

Release kinetic studies

In order to study the release mechanisms, some of the most relevant and commonly used mathematical models that describe the release curves. Higuchi, Korsmeyer-Peppas and zero order models were used to fit the experimental data using non-linear and linear regression. The results were compared in terms of goodness of the fit.

The Higuchi model (Eq. 4) was initially used to describe the release rate from planar polymer systems (35), and then it was extended to different polymeric geometries (36). This model has many assumptions, including perfect sink conditions throughout the experiment, initial drug concentration higher than drug solubility, and constant drug diffusivity (37).

$$M_t/M_\infty = A + k_H.t^{1/2} \qquad (4)$$

where M_t/M_∞ is the fractional release of drug at time t (M_t and M_∞ are the amount of drug released at time t, and at infinite time, respectively), K_H is the kinetic constant that include design characteristics of the system, and A is a constant that represents the extension of the burst release.

The Korsmeyer-Peppas model (Eq. 5) is also widely used for its simplicity to fit the first 60% of the release data:

$$M_t/M_\infty = A + k_{KP}.t^n \qquad (5)$$

where A is a constant that represents the extension of the burst release, and K_{KP} is the kinetic constant that include design characteristics of the system, and n is the release exponent, that characterize the mechanism of drug release.

Zero order model (Eq. 6) considers that the diffusion rate of the drug is constant and independent of the amount of encapsulated drug, in polymer systems showing neither swelling nor disintegration.

$$M_t/M_\infty = A_S + k.t \qquad (6)$$

where A_S is the initial amount of drug in the solution and k is the kinetic constant. This model describes the release data of the osmotic and reservoir drug release systems.

Statistical analysis

All the fiber diameters are expressed as mean ± standard deviation. Statistical differences between the fiber

diameters of the scaffolds were determined by performing a Student's test with the confidence interval of 99% ($p \leq 0.01$).

Data of embelin content and release measurements are expressed as mean ± standard deviation. The statistical differences were determined by applying the Student's test with a confidence interval of 95% ($p \leq 0.5$).

Results and discussion

Physicochemical and morphological characterization of nanofibrous scaffolds

In electrospinning process, the mean diameter and morphology of micro/nanofibers of electrospun scaffolds are strongly dependent of intrinsic properties of polymeric solution, processing parameters and ambient conditions (38,39). Solvents and solvent mixtures used in polymeric solutions for electrospinning have an important role in many aspects of the process. Solubility of polymeric chains and bioactive agents, facility of transporting conductive charges, and solidification rate are dependent of solvent properties (boiling point, dipole moment, dielectric constant, conductivity). Furthermore, these properties are crucial for the formation of electrospun fibers. In this work, these parameters were precisely controlled, and numerous experiments were carried out with the purpose of obtaining uniform bead-free continuous nanofibers (24,40).

PCL-based scaffolds were successfully prepared by electrospinning technique. The morphology of samples, as examined by SEM, are shown in Fig. 1.

The selected experimental conditions allowed the generation of continuous and uniform fibers. The surface of PCL samples displayed a typical electrospun structure of randomly oriented fibers and interconnected pores. The incorporation of embelin in the polymeric matrix led to uniform and smooth fiber surfaces. In a previous work, Cortez Tornello et al. (24) reported that the use of dichloromethane/methanol solvent mixture produced the formation of needle-like structures on surface that can be ascribed to the presence of a small fraction of crystallized embelin. However, no evidences of those surface morphologies were found when DCM:DMF (1:1) was used.

Mean diameters were in the range of 300 nm (PCL: 274 ± 90 nm; $PCLE_{1.5}$: 276 ± 80 nm, $PCLE_3$: 287 ± 90 nm and $PCLE_5$: 296 ± 90 nm). The use of DMF in the solvent mixture with DCM led to the formation of fibers with diameters four times lower than the observed with DCM: methanol (24). The dipole moment of DMF (3.86 D) and boiling point (153°C) compared with the ones of methanol (1.70 D and 65°C) are responsible for the higher electrical susceptibility and lower fiber diameter. Diameter distributions of PCL and PCLE nanofibers are shown in Fig. 2. No significant variation on mean diameter values and its distribution in PCL fibers with embelin incorporation.

Surface composition of scaffolds was studied by ATR-FTIR considering samples with the highest embelin content ($PCLE_5$) (spectra shown in supplementary material, Fig. S1). Embelin exhibited characteristic peaks at 3300 cm^{-1} (υO-H; 2918 cm^{-1} and 2848 cm^{-1} (υaC-H and

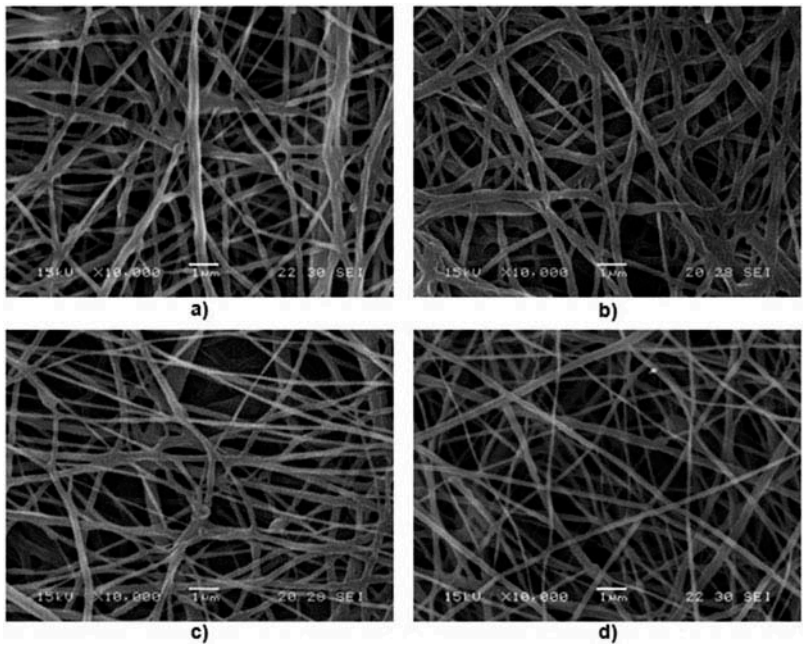

Figure 1. SEM micrographs of electrospun scaffolds (Magnification 10000×), a) PCL, b) PCLE1.5, c) PCLE3 and d) PCLE5.

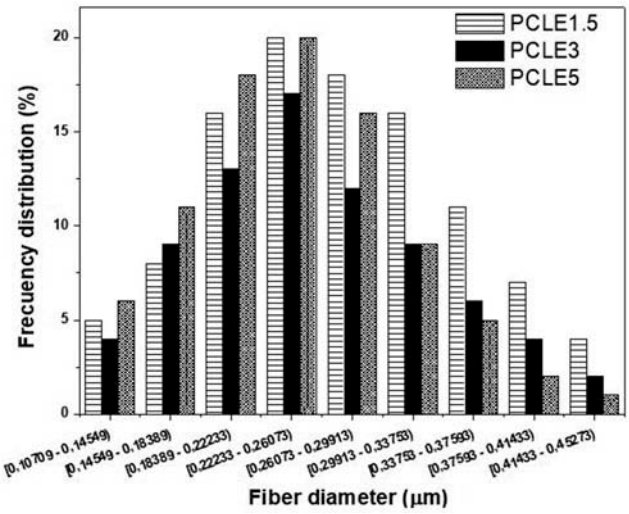

Figure 2. Diameter frequency distribution of PCLE nanofibers with different embelin content.

υsC-H in CH_2), and 1612 cm^{-1} (υC=C), 1462 cm^{-1} (δC-H in $-CH_2$), 1375 cm^{-1} (δC-H in $-CH_3$), 1219 cm^{-1}, (υC=O). PCL spectra exhibited the typical signals of polyesters at 2943 and 2864 cm^{-1} (υaC-H and υsC-H in CH_2), 1720 cm^{-1} (υC=O in ester), 1398 cm^{-1} and 1368 cm^{-1} (δC-H in CH_2), 1246 cm^{-1} and 1194 cm^{-1} (υC-O-C in ester), and 1108 cm^{-1} (υC-O-C in ether) (25).

Surface composition of electrospun scaffolds (PCL and PCLE) was determined by XPS analysis. PCL surface shows the presence of carbon (C1s, 285 eV) and oxygen (O1s, 532 eV) (Fig. 3 and supplementary material, Fig. S2).

The C1*s* peak was fitted with three components that correspond to species C*-C y C*-H (285 eV), C*-O (286,3 eV) y C*(=O)O (289 eV) (41). On the other hand, O1s peak was fitted with two components that correspond to species C=O* y C(=O)O*. All samples showed an energy band to approximately at 102.2 eV that correspond to Si2p, and this band can be attributed to low silicon contamination (<1%). Surface area relationships were determined from C1*s* and O1*s* signal values, considering that the area value was divided by the product of Scofield factor (RSF), transmission factor and mean free path (MFP). The relationship C1*s*/O1*s* (3.33/1) was slightly higher than the theoretical value (3/1), due to the presence of a greater amount of adventitious carbon (42). $PCLE_3$ scaffolds showed a slightly higher atomic relationship C1*s*/O1*s* with respect to the one of PCL (1.02), and could be attributed to the presence of embelin at the fiber surface. $PCLE_5$ samples presented a highest C1*s*/O1*s* atomic ratio (1.07), in agree with a higher embelin concentration.

Thermal properties and crystallinity

Thermal properties, as determined by DSC, are summarized in Table 1, while that DSC thermograms are presented in supplementary material (Fig. S3). Embelin displayed three characteristic melting endotherms (24). Embelin melting peaks were suppressed in PCLE scaffolds, indicating a very good dispersion of embelin in the PCL matrix. Embelin incorporation led to the increase in PCL crystallinity with the increase of embelin content. Therefore, it is evident that the presence of embelin favored the ordering of PCL chains (Table 1). The chemical structure of embelin has a chain of 10 methylene groups that could interact with PCL macromolecular

Table 1. Thermal properties of embelin and scaffolds.

Sample	T_m (°C)	ΔH_m (J.g^{-1})	X_{cPCL} (%)	ΔH_{mE} (J.g^{-1})	X_{cE} (%)
PCL	61.13	71.36	48.20	-	-
$PCLE_5$	58.97	78.76	53.20	-	-
$PCLE_3$	59.53	76.39	51.60	-	-
$PCLE_{1.5}$	59.89	73.58	49.70	-	-
Embelin	81.70; 87.10 145.80	-	-	63.45 129.68	100

Abbreviations: ΔH_m, melting heat; ΔH_{mE}, melting heat of embelin; T_m, melting temperature; X_{cPCL}, degree of crystallinity of PCL; X_{cE}, degree of crystallinity of embelin.

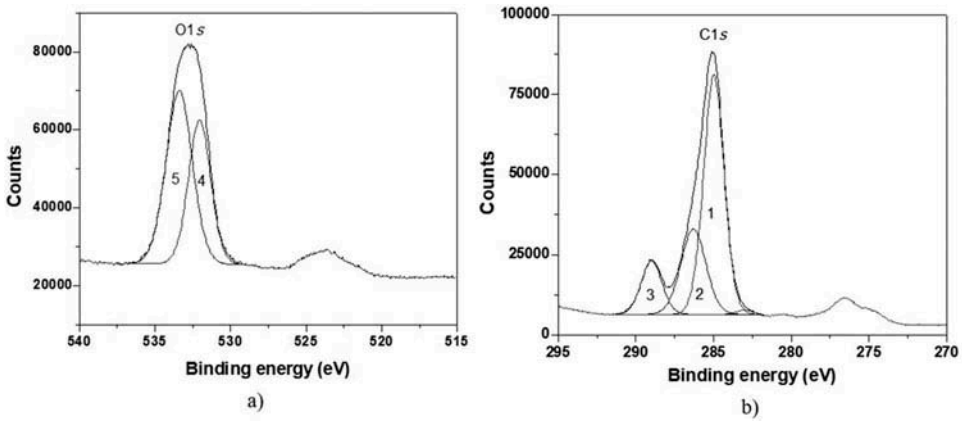

Figure 3. XPS spectrum of PCL, a) C1s region, b) O1s region.

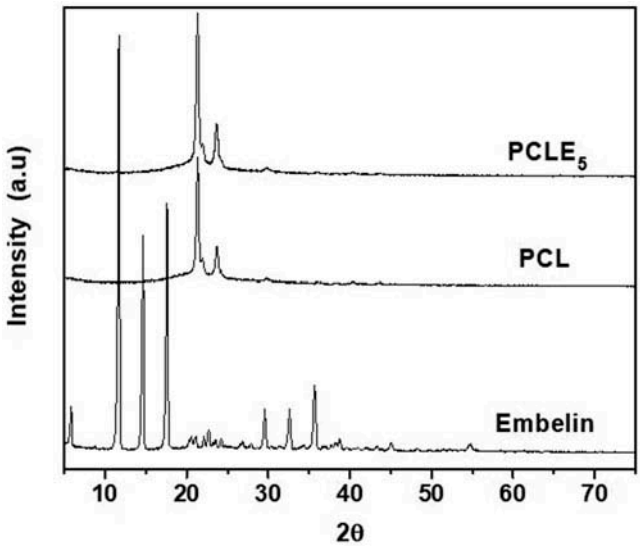

Figure 4. XRD patterns of embelin and electrospun scaffolds.

chains through dispersive interactions, allowing crystallize a higher fraction of PCL.

XRD diffractograms of embelin, and electrospun PCLE and PCLEA scaffolds are shown in Fig. 4. Embelin exhibited several intense peaks at 2θ = 5.81°, 11.70°, 14.63°, 17.59°, 29.53°, 32.63°, and 35.69°. However, these peaks were not observed in the XRD patterns of PCLE scaffolds. This indicates that the embelin could be molecularly dispersed within the polymer, distributed in an amorphous state or in crystalline state with very small size, as noted in the thermal and XPS analysis. The patterns of electrospun scaffolds correspond to characteristic peaks showed by PCL (2θ = 21.40° and 23.75°).

Drug loading capacity and encapsulation efficiency

Table 2 shows the embelin content in PCLE and multilayer scaffolds per mass unit of sample (M_E), loading capacity (LC), and encapsulation efficiency (EE). LC values of $PCLE_5$ (4.8%), $PCLE_3$ (2.8%), and $PCLE_{1.5}$ (1.4%) scaffolds showed that embelin content were slightly lower than the amount present in the polymeric solution. On the other hand, EE values did not show significant variation (94 to 96%). These values were close to reported for PCL electrospun fibers with timolol loaded for glaucoma treatment (95.2%) (43), and higher than the reported values for PCL fibers with nervous grown factor (NGF) (88.6%) and PCL fibers with camptothecin for cancer treatment (59%) (44,45).

Table 2. Embelin content incorporated in PCLE and multilayered scaffolds per mass unit of sample (M_E), loading capacity (LC), and encapsulation efficiency (EE).

Scaffold	M_E (± s.d.) (mg g^{-1})	LC (± s.d.) (%)	EE (± s.d.) (%)
$PCLE_{1.5}$	13.94 ± 0.59	1.39 ± 0.12	94.26 ± 0.02
$PCLE_3$	27.58 ± 0.41	2.76 ± 0.11	96.32 ± 0.03
$PCLE_5$	48.00 ± 0.61	4.80 ± 0.12	95.14 ± 0.03
B10	13.85 ± 0.45	1.38 ± 0.11	96.32 ± 0.03
B60	9.34 ± 0.57	0.93 ± 0.11	96.32 ± 0.04
T10	7.72 ± 0.34	0.77 ± 0.12	96.32 ± 0.03
T60	5.75 ± 0.23	0.58 ± 0.11	96.32 ± 0.04

$PCLE_3$ scaffold showed the highest EE value and a LC value that indicates the almost complete incorporation of initial embelin content of polymeric solution. For this reason, $PCLE_3$ was selected as drug-loaded mesh for the preparation of multilayered scaffolds. Thus, the EE values of multilayered scaffolds were equal to the calculated ones for $PCLE_3$ mesh (96%), while that LC values decreased as a consequence of the presence of additional fibrous layers.

Study of the release behavior from PCLE scaffolds and multilayered structure

Effect of embelin concentration and pH buffer solution

Figure 5 shows the *in vitro* release profiles of PCLE scaffolds with different embelin content ($PCLE_5$, $PCLE_3$ and $PCLE_{1.5}$) in PBS (pH = 7.4) and PCB (pH = 5.0) at 37°C.

The release profiles of PCLE scaffolds revealed that embelin can released from PCL matrix to the aqueous solutions with pH 7.4 and 5. Two clearly distinguished stages were identified in the release process. In a first stage, a high release rate was observed, normally known as burst effect. One suggested explanation for the burst effect in monolithic systems is that some drug becomes trapped on the surface of the polymer matrix during manufacturing process, and is released immediately upon activation in a release medium (26). Migration of drugs solvent evaporation may result in a heterogeneous distribution of drug in the polymer matrix that contributes to this effect. PCL degradation was not involved in the release process because that the hydrolytic degradation time of PCL is very long (several months) compared with *in vitro* release time (46). Since the absorption of medium by PCL in 10 h is less than 0.5%, swelling effects werenot considered (46). In the second stage, a diffusion-controlled mechanism was observed.

The release profile of embelin from $PCLE_5$ in PBS showed a burst release during a first 12 h, where 88% of the drug was released and the remaining one in 96 h (4 days) (Fig. 5a). In PCB, burst effect release at 12 h was 57%, completing the release in 10 days (Fig. 5b). The result show that the first stage of burst release presented an evident dependence of pH in both scaffolds, being lower in PCB solution and the same time more prolonged in the time.

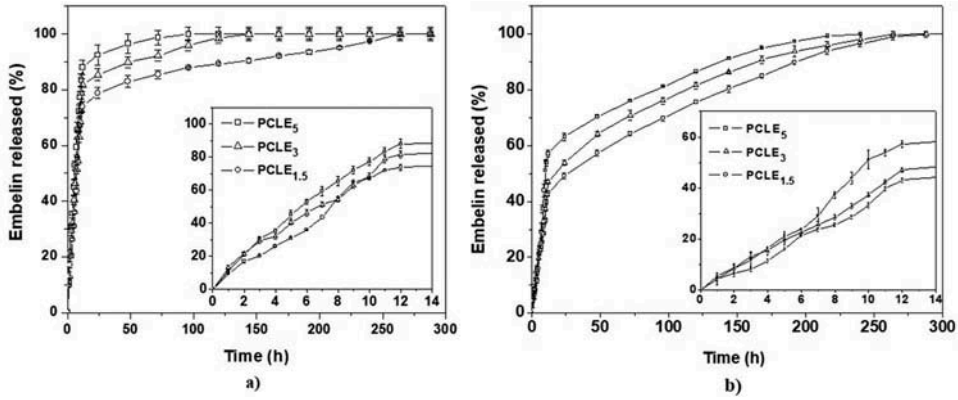

Figure 5. Release profiles of embelin from scaffolds with different embelin content: PCLE5, PCLE3 and PCLE1.5 in a) PBS (pH = 7.4) and b) PCB (pH = 5.0).

Figure 5 also shows that the initial embelin release in PCB was lower than in PBS. These results indicate that embelin initial release are dependent of pH buffer solution and agent bioactive solubility. Results show that the release profiles of the scaffolds can be modulated, within certain limits, depending of embelin content present on electrospun scaffolds.

Effect of multilayered structure and pH buffer solution

Figures 6 and 7 shows embelin release profiles at 37°C from $PCLE_3$ and multilayered scaffolds in PBS and PCB, respectively.

Embelin content in multilayered meshes was equal to the present in $PCLE_3$. As can be clearly seen, hydrophobic PCL layers produced an important decrease in the amount of embelin released in the initial stage. The reduction increased with the increase of thickness or number of additional PCL layers, following the order B10, B60, T10, and T60. This effect could be associated to two phenomena. The entry of buffer medium, which is delayed by the presence of additional PCL hydrophobic layers, and the embelin diffusion towards the release medium, which it is also slowed. In PBS, percentage of embelin released in 12 h was reduced in 67.3% for B60 and 88.9% in T60. In PCB, a decrease of 49.6% in B60 and 84.6% in T60 respect to $PCLE_3$ was observed. Recently, Lavielle et al. (47) reported the release behavior of sandwich-like structure with nanoparticle-loaded nanofibers and hydrophobic or hydrophilic layers for temporal drug delivery. They used confined dye-loaded meshes and tailored the release profiles in PBS. The authors found that burst release was completely avoided and a delayed release was observed. This could be due to the higher thickness of sheath layers (12 μm) compared with the layers obtained at 60 min deposition (2 μm). Our results show that it is possible to modulate the system release profile by controlling the number and thickness of electrospun layers over the loaded-scaffolds, acting this multilayered scaffold as a reservoir of embelin.

Kinetic analysis of in vitro release profiles

The kinetic analysis of the embelin release process at different pH from PCLE scaffolds was carried out, and the parameters derived from fitting models of release

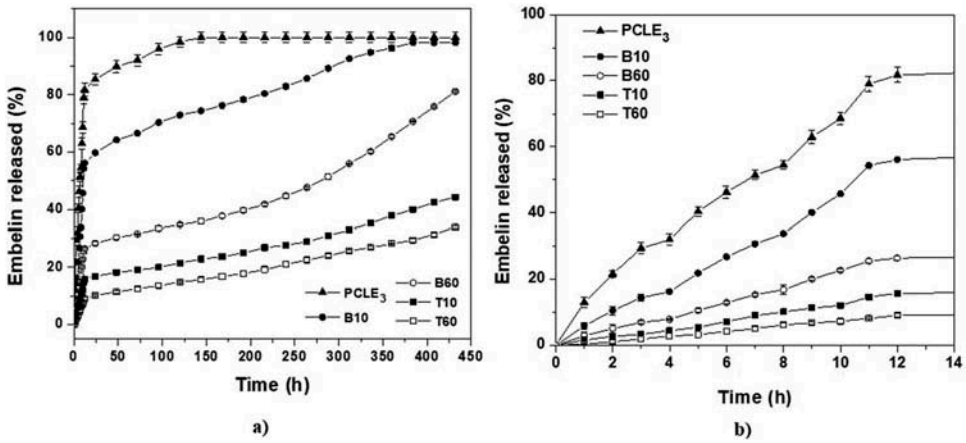

Figure 6. Release profiles of embelin from PCLE3, B10, B60, T10 and T60 in PBS (pH = 7.4) during a) 450 h and b) first 14 h.

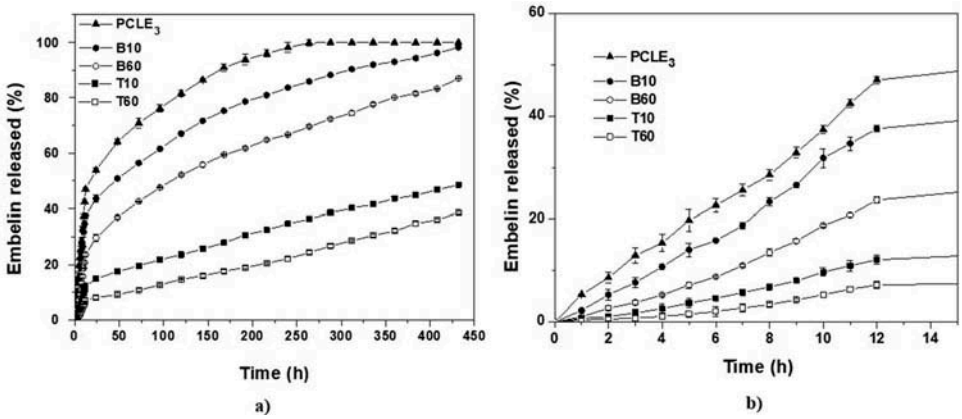

Figure 7. Release profiles of embelin from PCLE3, B10, B60, T10 and T60 in PCB (pH = 5.0) during a) 450 h and b) first 14 h.

Table 3. Parameters of release profiles from PCLE series and multilayered scaffolds in PBS (pH = 7.4) and PCB (pH = 5.0).

			Higuchi model		Korsmeyer-Peppas model		
Buffer	Scaffold	t[a] (h)	K_H ($h^{-1/2}$) (s.d.)	R^2	K_{KP} (h^{-n}) (s.d.)	n (s.d.)	R^2
PBS	$PCLE_{1.5}$	10	2.058 (0.052)	0.945	4.359 (0.372)	0.354 (0.016)	0.990
	$PCLE_3$	10	2.994 (0.227)	0.780	9.737 (0.766)	0.231 (0.018)	0.984
	$PCLE_5$	12	1.334 (0.022)	0.996	1.385 (0.213)	0.491 (0.037)	0.994
	B10	10	2.538 (0.105)	0.905	6.676 (0.666)	0.299 (0.021)	0.983
	B60	10	22.76	0.967	1.445 (0.342)	0.466 (0.048)	0.965
	T10	10	12.09	0.941	1.494 (0.380)	0.408 (0.052)	0.945
	T60	12	9.05	0.856	0.029 (0.006)	1.110 (0.034)	0.994
PCB	$PCLE_{1.5}$	12	2.389 (0.041)	0.988	1.746 (0.256)	0.564 (0.030)	0.992
	$PCLE_3$	12	3.332 (0.051)	0.986	2.569 (0.389)	0.550 (0.051)	0.988
	$PCLE_5$	12	2.854 (0.068)	0.975	1.526 (0.253)	0.625 (0.068)	0.990
	B10	9	3.655 (0.037)	0.990	5.421 (0.267)	0.429 (0.008)	0.997
	B60	9	3.411 (0.010)	0.999	3.535 (0.113)	0.493 (0.006)	0.999
	T10	9	1.806 (0.032)	0.976	0.766 (0.092)	0.653 (0.021)	0.993
	T60	9	1.354 (0.051)	0.910	0.133 (0.027)	0.912 (0.035)	0.989

		Stage 2, zero order			Stage 3, zero order		
Buffer	Scaffold	t_o (h)	t_f (h)	R^2	t_o (h)	t_f (h)	R^2
PBS	B10	-	-	-	182	384	0.989
	B60	-	-	-	240	432	0.967
	T10	-	-	-	264	432	0.994
	T60	12	432	0.995	-	-	-
PCB	B10	-	-	-	-	-	-
	B60	-	-	-	-	-	-
	T10	24	432	0.994	-	-	-
	T60	12	432	0.998	-	-	-

[a]Starting time of the second stage.

mechanisms to experimental data of the second stage are listed in Table 3. Higuchi and Korsmeyer-Peppas mathematical models were tested through non-linear least-square curve fitting.

Korsmeyer-Peppas model showed the best-fit curve for PCLE scaffolds in the investigated mediums. The constant K_{KP} and n are characteristics of the drug-polymer system, while that the diffusional exponent is dependent on the geometry of the sample and the physical mechanisms of release. A Fickian diffusion ($n = 0.491$) was observed from $PCLE_5$ in PBS, and in this case the Korsmeyer-Peppas model is equivalent to the Higuchi model (square root model). The mechanism in PCB was anomalous transport or non-Fickian diffusion for $PCLE_5$. In this case, the mechanism experienced a deviation respect to Fickian diffusion, where coexist a term of Fickian contribution ($K_1 t^{0.5}$) and a zero-order term ($K_2 t$). In $PCLE_3$ and $PCLE_{1.5}$ scaffolds, embelin release was quasi-Fickian in PBS and presented an anomalous transport mechanism in PCB.

In case of B10 scaffolds, embelin diffusional stage was partially fitted with Korsmeyer-Peppas model in PBS, up to 182 h approximately. After that, it was possible identify a second stage that fitted with a zero-order model until the complete release. On the other hand, embelin release profile in PCB was completely fitted with Korsmeyer-Peppas model.

B60 scaffolds also showed the same behavior in PBS. The diffusional stage was fitted with Korsmeyer-Peppas model (up to 240 h) and a second stage of zero order, and in PCB all range was fitted with Korsmeyer-Peppas (n near to 0.5) that correspond to Higuchi model. This asymmetric scaffold differs from present in a transdermal drug delivery system, in which the release occurs from only one side of the membrane. PCL nanofibrous layer in B10 and B60 did not constitute a barrier for preventing the embelin release.

T10 scaffolds also showed a diffusional stage fitted with Korsmeyer-Peppas model and a second stage of zero order. In PCB, the diffusional stage was fitted with Korsmeyer-Peppas model (n near to 1) that

correspond to the release zero order model until total release. Finally, T60 scaffolds exhibited a diffusional stage fitted with Korsmeyer-Peppas model (n near to 1) in both release mediums, that correspond to the zero-order model. Peppas defined to this behavior as non-Fickian diffusion or case II transport (48).

These multilayer scaffolds have characteristics enough to produce a drug delivery system that present a release profile with a constant drug release rate.

Conclusions

Embelin-loaded poly(ε-caprolactone) electrospun nanofibrous scaffolds were prepared were prepared from polymer solutions by electrospinning technique, varying the amount of incorporated embelin. Embelin content did not alter the morphology nor mean diameter of the nanofibers, while that the crystallinity of PCL showed an increase.

In vitro embelin release from PCLE scaffolds displayed profiles with a high initial release, followed by a slow diffusional phase. The process depended on the pH, embelin content and the solvent mixture of the initial solution. The modeling of release data implied a two-stage release mechanism: a fast dissolution phase (mainly produced by amorphous drug located at the surface) and a diffusion phase. The kinetic analysis results showed that the Korsmeyer-Peppas model fitted very well to the experimental data of the diffusion phase for the investigated scaffolds and pH.

Multilayered scaffolds (bi- and three-layers) were prepared as a strategy to modulate release profiles and decrease or avoid the initial embelin release. The results showed that it is possible to modulate the release profile depending on the number and thickness of layers added to $PLCE_3$ scaffold that acts as an embelin reservoir. Three-layered scaffolds acted as a reservoir-type drug delivery system, with a bioactive agent contained in the nanofibrous core in a sandwich-like nanofibrous sheath layer. The PCL layers exerted a control over the release process and the three-layered mesh exhibited efficient sustained drug delivery with no burst release.

In summary, electrospun multilayered scaffolds containing embelin presented characteristics, morphology and release profiles that could be very attractive for use as embelin controlled release systems.

Acknowledgments

P.R.C.T. thanks to CONICET for the fellowship awarded.

Funding

This work was supported by the Argentinean National Agency of Scientific and Technological Promotion (grant PICT 224), National University of Mar del Plata (grant 15/G479), CONICET (grant PIP 0089), and PIO CONICET-SECITI (N° 0022 2015) and CICITCA (UNSJ, Argentina).

References

1. Kenry, and Lim, C.T. 2017 Nanofiber technology: current status and emerging developments. *Progress in Polymer Science*, 70:1–7.
2. Caracciolo, P.C., Cortez Tornello, P.R., Montini Ballarin, F., and Abraham, G.A. 2013 Development of electrospun nanofibers for biomedical applications: state of the art in latin america. *Journal Biomaterials Tissue Engineering*, 3:39–60.
3. Agarwal, A., Wendorff, J.H., and Greiner, A. 2009 Progress in the field of electrospinning for tissue engineering aplications. *Advancement Materials*, 21:3343–3351.
4. Dahlin, R.L., Kasper, F.K., and Mikos, A.G. 2011 Polymeric nanofibers in tissue engineering. *Tissue Engineering B-Reviews*, 17:349–364.
5. Suryani, S., Nazli Naim, M., Wuled Lenggoro, I., Mokhtarc, M.N., Bakar, N.F.A., and Gen, M. 2016 Immobilisation of cyclodextrin glucanotransferase into polyvinyl alcohol (PVA) nanofibres via electrospinning. *Biotechnology Reports*, 10:44–48.
6. Caracciolo, P.C., Rial-Hermida, M.I., Montini-Ballarin, F., Abraham, G.A., Concheiro, A., and Álvarez-Lorenzo, C. 2017 Surface-modified bioresorbable electrospun scaffolds for improving hemocompatibility of vascular grafts. *Materials Sciences Engineering C*, 75:1115–1127.
7. Liu, X., Lin, T., Fang, J., Yao, G., Dodson, M., and Wang, X. 2010 In vivo wound healing and antibacterial performances of electrospun nanofibre membranes. *Materials Research A*, 94:499–508.
8. Thakur, R.A., Florek, C.A., Kohn, J., and Michniak, B. B. 2008 Electrospun nanofibrous polymeric scaffold with targeted drug release profiles for potential application as wound dressing. *International Journal Pharmaceutical*, 94(2008):87–93.
9. Montini-Ballarin, F., Calvo, D., Caracciolo, P.C., Rojo, F., Frontini, P.M., Abraham, G.A., and Guinea-Totuero, G. 2016 Mechanical behavior of bilayered small-diameter nanofibrous structures as biomimetic vascular grafts. *Journal Mechanisms Behavioral Biomedical Materials*, 60:220–233.
10. Woods, I., and Flanagan, T.C. 2014 Electrospinning of biomimetic scaffolds for tissue-engineered vascular grafts: threading the path. *Expert Reviews Cardiovascular Therapeutics*, 12:815–832.
11. Montini Ballarin, F., Caracciolo, P.C., Blotta, E., Ballarin, V.L., and Abraham, G.A. 2014 Optimization of poly(L-lactic acid)/segmented polyurethane electrospinning process for the production of bilayered small-diameter nanofibrous tubular structures. *Materials Sciences and Engineering C*, 42:489–499.

12. Zamani, M., Prabhakaran, M.P., and Ramakrishna, S. 2013 Advances in drug delivery via electrospun and electrosprayed nanomaterials. *International Journal Nanomedicine*, 8:2997–3017.
13. Sill, T.J., and Von Recum, H.A. 2008 Electrospinning: applications in drug delivery and tissue engineering. *Biomaterials*, 29:1989–2006.
14. Hu, X., Liu, S., Zhou, G., Huang, Y., Xie, Z., and Jing, X. 2014 Electrospinning of polymeric nanofibers for drug delivery applications. *Journal Control Release*, 185:12–21.
15. Pados, G., Makedos, A., and Tarlatzis, B. 2013 Adhesion prevention strategies in laparoscopic surgery, in: Amornyotin, S Ed., *Endoscopy*; InTech: Rijeka, Croatia, 49–72.
16. Bölgen, N., Vargel, I., Korkusuz, P., Menceloglu, Y.Z., and Piskin, E. 2007 In vivo performance of antibiotic embedded electrospun PCL membranes for prevention of abdominal adhesions. *Journal of Biomedical Materials Research Applications Biomaterials*, 81:530–543.
17. Bhardwaj, N., and Kundu, S.C. 2010 Electrospinning: a fascinating fiber fabrication. *Biotechnology Advances*, 3:325–347.
18. Kenawy, E.-R., Abdel-Hay, F.I., El-Newehy, M.H., and Wnek, G.E. 2009 Processing of polymer nanofibers through electrospinning as drug delivery systems. *Materials Chemistry and Physics*, 1:296–302.
19. Haq, K., Ali, A., and Siddiqui, A.W. 2005 New compounds from the seeds of Embelia ribes burm. *Pharmazie*, 60:69–71.
20. Feresin, G.E., Tapia, A., Sortino, M., Zacchino, S., De Arias, A.R., Inchausti, A., Yaluff, G., Rodriguez, J., Theoduloz, C., and Schmeda-Hirschmann, G. 2003 Bioactive alkyl phenols and embelin from Oxalis erythrorhiza. *Journal Ethnopharmacol*, 88:241–247.
21. Poojari, R. Embelin a drug of antiquity: shifting the paradigm towards modern medicine. *Expert Opinion Investigations Drugs*, 3:427–444.
22. Peña, R., Martín, P., Feresin, G.E., Tapia, A., Machín, F., and Estévez-Braun, A. 2016 Domino synthesis of embelin derivatives with antibacterial activity. *Journal of Natural Products*, 79:970–977.
23. Raghunathan, K., and Mitra, R. 1999 *Pharmacognosy of Indigenous Drugs*; Central Council for Research in Ayurveda and Siddha: New Delhi, India, 1046–1061.
24. Cortez Tornello, P.R., Feresin, G.E., Tapia, A., Veiga, I. G., Moraes, Â.M., Abraham, G.A., and Cuadrado, T.R. 2012 Dispersion and release of embelin from electrospun, biodegradable, polymeric membranes. *Journal of Polymer*, 44:1105–1111.
25. Cortez Tornello, P.R., Tapia, A., Feresin, G.E., Dzieciuch, M., Cuadrado, T.R., and Abraham, G.A. 2017 Effect of processing techniques on new PCL-embelin microparticles of biomedical interest. *Advancement Polymer Technical*, doi:10.1002/adv.21814.
26. Meinel, A.J., Germershaus, O., Luhmann, T., Merkle, H.P., and Meinel, L. 2012 Electrospun matrices for localized drug delivery: current technologies and selected biomedical applications. *European Journal Pharmaceutical Biopharmaceuticals*, 81:1–13.
27. Huang, X., and Brazel, C.S. 2001 On the importance and mechanisms of burst release in matrix-controlled drug delivery systems. *Journal Control Release*, 73:121–136.
28. Karataş, A., Algan, A.H., Pekel-Bayramgil, N., Turhan, F., and Altanlar, N. 2016 Ofloxacin loaded electrospun fibers for ocular drug delivery: effect of formulation variables on fiber morphology and drug release. *Current Drug Delivery*, 13:433–443.
29. Chou, S.-F., and Woodrow, K.A. 2017 Relationships between mechanical properties and drug release from electrospun fibers of PCL and PLGA blends. *Journal Mechanisms Behavioral Biomedical Materials*, 65:724–733.
30. Duque Sánchez, L., Brack, N., Postma, A., Pigram, P. J., and Meagher, L. 2016 Surface modification of electrospun fibres for biomedical applications: a focus on radical polymerization methods. *Biomaterials*, 106:24–45.
31. Yao, J., Zhang, S., Li, W., Dua, Z., and Li, Y. 2016 In vitro drug controlled-release behavior of an electrospun modified poly(lactic acid)/bacitracin drug delivery system. *RSC Advancement*, 6:515–521.
32. Chitra, M., Sukumar, E., Suja, V., and Devi, C.S. 1994 Antitumor, anti-inflammatory and analgesic property of embelin, a plant product. *Chemotherapy*, 40:109–113.
33. Radhakrishnan, N., Gnanamani, A., and Mandal, A.B. 2011 A potential antibacterial agent embelin, a natural benzoquinone extracted from Embelia ribes. *Biologic Medica*, 3:1–7.
34. Van Krevelen, W., and Te Nijenhuis, K. 2009 *Properties of Polymers*; 4th edn, Elsevier: Amsterdam, The Netherlands, 121.
35. Higuchi, T. 1961 Rate of release of medicaments from ointment bases containing drugs in suspensions. *Journal Pharmaceutical Sciences*, 50:874–875.
36. Siepmann, J., and Siepmann, F. 2008 Mathematical modeling of drug delivery. *International Journal Pharmaceutical*, 364:328–343.
37. Grassi, M., and Grassi, G. 2005 Mathematical modelling and controlled drug delivery: matrix systems. *Current Drug Delivery*, 2:97–116.
38. Andrady, A.L. 2008 *Science and Technology of Polymer Nanofibers*; John Wiley & Sons Inc., New Jersey, USA.
39. Bosworth, L.A., and Downes, S. 2011 *Electrospinning for Tissue Regeneration*; Woodhead Publishing: Oxford, London.
40. Cortez Tornello, P.R., Caracciolo, P.C., Cuadrado, T.R., and Abraham, G.A. 2014 Structural characterization of electrospun micro/nanofibrous scaffolds by liquid extrusion porosimetry: a comparison with other techniques. *Materials Sciences Engineering C*, 41:335–342.
41. Louette, P., Bodino, F., and Pireaux, -J.-J. 2005 Poly (caprolactone) (PCL) XPS reference core level and energy loss spectra. *Surface Science Spectra*, 12:27–31.
42. Luk, J.Z., Cooper-White, J., Rintoul, L., Taran, E., and Grondahl, L. 2013 Functionalised polycaprolactone films and 3D scaffolds via gamma irradiation induced grafting. *Journal of Materials Chemistry B*, 1:4171–4181.

43. Gagandeep, T.G., Malik, B., Rath, G., and Goyal, A.K. 2014 Development and characterization of nano-fiber patch for the treatment of glaucoma. *European Journal Pharmaceutical Sciences*, 464:243–251.
44. Valmikinathan, C.M., Defroda, S., and Yu, X. 2009 Polycaprolactone and bovine serum albumin based nanofibers for controlled release of nerve growth factor. *Biomacromolecules*, 10:1084–1089.
45. Amna, T., Barakat, N.A.M., Shamshi Hassan, M., Khil, M.-S., and Kim, H.Y. 2013 Camptothecin loaded poly (ε-caprolactone) nanofibers via one-step electrospinning and their cytotoxicity impact. *Colloids Surface A Physicochem Engineering Aspects*, 431:1–8.
46. Albertsson, A.C., and Varma, I.K. 2002 Aliphatic polyesters: synthesis, properties and applications. *Advancement Polymer Sciences*, 157:1–40.
47. Lavielle, N., Hébraud, A., Thöny-Meyer, L., Rossi, R.M., and Schlatter, G. 2017 3D composite assemblies of microparticles and nanofibers for tailored wettability and controlled drug delivery. *Macromol Materials Engineering*, doi:10.1002/mame201600458.
48. Kosmidis, K., Rinaki, E., Argyrakis, P., and Macheras, P. 2003 Analysis of Case II drug transport with radial and axial release from cylinders. *International Journal Pharmaceutical*, 254:183–188.